$ZZ\gamma$ and $Z\gamma\gamma$ couplings at linear e^+e^- collider energies with the effects of **Z** polarization and initial state radiation

S. Atağ* and İ. Şahin[†]

Department of Physics, Faculty of Sciences, Ankara University, 06100 Tandogan, Ankara, Turkey

The constraints on the neutral gauge boson couplings, $ZZ\gamma$ and $Z\gamma\gamma$, are investigated at linear e^+e^- collider energies through the $Z\gamma$ production with longitudinal and transverse polarization states of the final Z boson. Because of high energy of linear electron- positron beams, initial state radiation (ISR) considerably changes the production cross section. We obtain an increase in the cross section by a factor of 2-3 due to ISR for transverse polarization and by a factor of 10-100 for longitudinal polarization states depending on the energy.

We find the 95% C.L. limits on the CP conserving form factors h_3^Z , h_4^Z , h_3^γ and h_4^γ with integrated luminosity $500fb^{-1}$ and $\sqrt{s} = 0.5$, 1, 1.5 TeV energies. It is shown that the longitudinal polarization of the Z boson, together with ISR, can improve sensitivities by factors 2-3.

PACS numbers: 12.15.Ji, 12.15.-y, 12.60.Cn, 14.80.Cp

I. INTRODUCTION

The self interactions of the gauge bosons are consequences of the non-abelian structure of the electroweak sector of the Standard Model (SM). The study of the trilinear gauge boson couplings leads to important tests of electroweak interactions. Neutral gauge boson couplings $ZZ\gamma$ and $Z\gamma\gamma$ are not generated at tree level by the SM. Higher order loop level corrections are highly below the current experimental sensitivity [1]. Nevertheless, the new physics with energy scale above present experimental threshold might provide tree level neutral triple-gauge boson couplings. Deviation of the couplings from the expected values would indicate the existence of new physics beyond the SM. Therefore precision measurements of triple vector boson vertices will be the crucial tests of the structure of the SM.

For the process $e^+e^- \to Z\gamma$ it is convenient to study the anomalous neutral triple gauge couplings $Z\gamma Z^\star$ and $Z\gamma\gamma^\star$ which obey Lorentz and gauge invariance. Within the formalism of Ref. [1, 2] there are eight anomalous coupling parameters h_i^Z , h_i^γ (i=1,...,4) which are all zero in the standard model. Here we are interested in CP-even couplings that are proportional to h_3^V and h_4^V ($V=Z,\gamma$). The photon and the Z boson in the final state are considered as on-shell particles while the third boson at the vertex, the s-channel internal propagator, is of-shell. Due to partial wave unitarity constraints at high energies, an energy dependent form factor ansatz can be cosidered:

$$h_i^V(s) = \frac{h_{i0}^V}{(1+s/\Lambda^2)^3} \; ; \; i = 1,3$$
 (1)

$$h_i^V(s) = \frac{h_{i0}^V}{(1+s/\Lambda^2)^4} \; ; \; i = 2,4$$
 (2)

In this work we assume that new physics scale Λ is above the collision energy \sqrt{s} and we neglect the energy dependence of the form factors in the energy region we are interested in.

CP conserving anomalous $Z(p_1)\gamma(p_2)Z(p_3)$ vertex function can be written following the low energy parametrization of the residual effect from the effective lagrangian [1, 2]:

$$ig_e \Gamma_{Z\gamma Z}^{\alpha\beta\mu}(p_1, p_2, p_3) = ig_e \frac{p_3^2 - p_1^2}{m_Z^2} \left[h_3^Z \epsilon^{\mu\alpha\beta\rho} p_{2\rho} + \frac{h_4^Z}{m_Z^2} p_3^{\alpha} \epsilon^{\mu\beta\rho\sigma} p_{3\rho} p_{2\sigma} \right]$$
 (3)

where m_Z and g_e are the Z-boson mass and charge of the proton. The $Z\gamma\gamma$ vertex function can be obtained with the replacements:

$$\frac{p_3^2 - p_1^2}{m_Z^2} \to \frac{p_3^2}{m_Z^2}, \quad h_i^Z \to h_i^\gamma, \quad i = 3, 4 \tag{4} \label{eq:4}$$

^{*}atag@science.ankara.edu.tr

[†]sahin@science.ankara.edu.tr

The overall factor p_3^2 in the $Z\gamma\gamma^*$ vertex function originates from electromagnetic gauge invariance. Due to Bose statistics the $Z\gamma\gamma$ vertex vanishes identically if both photons are on shell (Yang's theorem) [3].

Previous limits on the $Z\gamma Z^{\star}$ and $Z\gamma\gamma^{\star}$ anomalous couplings have been provided by the Tevatron $|h_3^Z|<0.36$, $|h_4^Z|<0.05, |h_3^{\gamma}|<0.37$ and $|h_4^{\gamma}|<0.05$ [4] and the combination of four LEP experiments ALEPH, DELPHI, L3, OPAL $-0.20 < h_3^Z < 0.07, -0.05 < h_4^Z < 0.12, -0.049 < h_3^{\gamma} < 0.008$ and $-0.002 < h_4^{\gamma} < 0.034$ [5] at 95% C.L. . Based on the analysis of ZZ production at the upgraded Fermilab Tevatron and the CERN Large Hadron Collider (LHC) achievable limits on the $ZZ\gamma$ couplings ($f_4^Z, f_4^{\gamma}, f_5^Z, f_5^{\gamma}$) have been discussed [6, 9]. Research and development on linear e^+e^- colliders at SLAC, DESY and KEK have been progressing and the physics

Research and development on linear e^+e^- colliders at SLAC, DESY and KEK have been progressing and the physics potential of these future machines is under intensive study. In this paper, the process $e^+e^- \to Z\gamma$ with the final state $\ell^+\ell^-\gamma$ is investigated to search for $Z\gamma Z^*$ and $Z\gamma\gamma^*$ couplings. Because of the high energy of the incomig beams, initial state electromagnetic radiative corrections (ISR) are taken into account using the structure function method. Another important point is the polarization of the final state Z boson. In order to determine the Z polarization, we show that the angular distribution of the Z decay products, has a clear correlation with the helicity states of the Z boson.

II. CROSS SECTIONS AND ANGULAR CORRELATIONS FOR FINAL STATE FERMIONS

In this section, we present the cross section calculation via helicity amplitudes for the complete process $e^+e^- \to Z\gamma \to \ell^+\ell^-\gamma$ and describe angular distributions of final state fermions to see the correlations with the polarization states of Z boson. Let us start with the differential cross section

$$d\sigma(e^+e^- \to Z\gamma \to \ell^+\ell^-\gamma) = \frac{1}{2s}|M|^2 \frac{d^3p_3}{(2\pi)^3 2E_3} \frac{d^3p_4}{(2\pi)^3 2E_4} \frac{d^3k_2}{(2\pi)^3 2E_\gamma} (2\pi)^4 \delta^4(p_1 + p_2 - p_3 - p_4 - k_2) \tag{5}$$

where p_1, p_2 are the momenta of incoming leptons, p_3, p_4 are the momenta of outgoing fermions and k_2 is the momentum of outgoing photon. $|M|^2$ is the square of the full amplitude which is averaged over initial spins and summed over final spins. The helicity dependent full amplitude can be expressed as follows

$$|M(\sigma_1, \sigma_2; \sigma_3, \sigma_4, \lambda_\gamma)|^2 (2\pi)^4 \delta^4(p_1 + p_2 - p_3 - p_4 - k_2) = \int \frac{d^4k_1}{(2\pi)^4} |\sum_{\lambda_Z} M_a(\sigma_1, \sigma_2; \lambda_Z, \lambda_\gamma) D_Z(k_1^2) M_b(\lambda_Z; \sigma_3, \sigma_4)^2$$

$$(2\pi)^4 \delta^4(p_1 + p_2 - k_1 - k_2) (2\pi)^4 \delta^4(k_1 - p_3 - p_4)$$
(6)

where k_1 is the internal momentum of the Z boson propagator. σ_1, σ_2 are the incoming lepton helicities, $\sigma_3, \sigma_4, \lambda_{\gamma}$ are the outgoing fermion and photon helicities. For the summation over the intermediate Z boson polarization we take the helicity basis $\lambda_Z = +, -, 0$. Here $D_Z(k_1)$ is the Breit-Wigner propagator factor for the Z boson

$$D_Z(k_1) = \frac{1}{k_1^2 - M_Z^2 + iM_Z\Gamma_Z} \tag{7}$$

Here $M_a(\sigma_1, \sigma_2; \lambda_Z, \lambda_{\gamma})$ is the helicity amplitudes for $e^+e^- \to Z\gamma$ with on shell Z boson which are provided in the appendix. $M_b(\lambda_Z; \sigma_3, \sigma_4)$ is the decay amplitude of the Z boson which will be given later. Using the narrow width approximation differential cross section becomes

$$d\sigma(e^{+}e^{-} \to Z\gamma \to \ell^{+}\ell^{-}\gamma) = \frac{1}{2s} \frac{1}{(2M_{Z}\Gamma_{Z})} |\sum_{\lambda_{Z}} M_{a}(\lambda_{Z}) M_{b}(\lambda_{Z})|^{2}$$

$$\frac{d^{3}k_{1}}{(2\pi)^{3}2E_{Z}} \frac{d^{3}k_{2}}{(2\pi)^{3}2E_{\gamma}} (2\pi)^{4} \delta^{4}(p_{1} + p_{2} - k_{1} - k_{2})$$

$$\frac{d^{3}p_{3}}{(2\pi)^{3}2E_{3}} \frac{d^{3}p_{4}}{(2\pi)^{3}2E_{4}} (2\pi)^{4} \delta^{4}(k_{1} - p_{3} - p_{4})$$
(8)

Here $M_a(\lambda_Z)$ and $M_b(\lambda_Z)$ indicate average over initial lepton spins, summmation over final state fermion spins and photon. In the rest frame of the Z boson where the decay amplitudes are most simply expressed, we get

$$d\sigma(e^{+}e^{-} \to Z\gamma \to \ell^{+}\ell^{-}\gamma) = \frac{1}{2s} \frac{1}{((2\pi)^{2}16M_{Z}\Gamma_{Z})} |\sum_{\lambda_{Z}} M_{a}(\lambda_{Z})M_{b}(\lambda_{Z})|^{2}$$

$$\frac{d^{3}k_{1}}{(2\pi)^{3}2E_{Z}} \frac{d^{3}k_{2}}{(2\pi)^{3}2E_{\gamma}} (2\pi)^{4}\delta^{4}(p_{1} + p_{2} - k_{1} - k_{2})$$

$$d\cos\theta^{\star}d\phi^{\star}$$
(9)

where θ^* and ϕ^* are the polar and azimuthal angles of the final state leptons in the Z rest frame with respect to the Z boson direction in the $\ell\ell\gamma$ rest frame. After integration over azimuthal angles ϕ^* interference terms will vanis as below

$$d\sigma(e^{+}e^{-} \to Z\gamma \to \ell^{+}\ell^{-}\gamma) = \frac{1}{2s} \frac{1}{(32\pi M_{Z}\Gamma_{Z})} [|M_{a}(+)M_{b}(+)|^{2} + |M_{a}(-)M_{b}(-)|^{2} + |M_{a}(0)M_{b}(0)|^{2}]$$
$$\frac{d^{3}k_{1}}{(2\pi)^{3}2E_{Z}} \frac{d^{3}k_{2}}{(2\pi)^{3}2E_{\gamma}} (2\pi)^{4}\delta^{4}(p_{1} + p_{2} - k_{1} - k_{2})d\cos\theta^{*}$$
(10)

This can be written in a more compact form

$$d\sigma(e^{+}e^{-} \to Z\gamma \to \ell^{+}\ell^{-}\gamma) = \frac{1}{(32\pi M_{Z}\Gamma_{Z})} \left[|d\sigma_{1}(+)|M_{b}(+)|^{2} + d\sigma_{1}(-)|M_{b}(-)|^{2} + d\sigma_{1}(0)|M_{b}(0)|^{2} \right] d\cos\theta^{\star}$$
(11)

If one performs further integration over polar angle $\cos \theta^*$ it turns out to be a well known result

$$d\sigma(e^{+}e^{-} \to Z\gamma \to \ell^{+}\ell^{-}\gamma) = [d\sigma_{1}(+) + d\sigma_{1}(-) + d\sigma_{1}(0)]BR(Z \to \ell^{+}\ell^{-})$$
$$= d\sigma_{1}(e^{+}e^{-} \to Z\gamma)BR(Z \to \ell^{+}\ell^{-})$$
(12)

Explicit forms of the decay amplitudes $|M_b(+)|^2$, $|M_b(-)|^2$ and $|M_b(0)|^2$ in the Z rest frame are given by

$$|M_b(+)|^2 = \frac{M_Z^2}{2} [g_L^2 (1 - \cos \theta^*)^2 + g_R^2 (1 + \cos \theta^*)^2]$$
(13)

$$|M_b(-)|^2 = \frac{M_Z^2}{2} [g_L^2 (1 + \cos \theta^*)^2 + g_R^2 (1 - \cos \theta^*)^2]$$
(14)

$$|M_b(0)|^2 = M_Z^2(g_L^2 + g_R^2)\sin^2\theta^*$$
(15)

$$|M_b(0)|^2 = M_Z^2 (g_L^2 + g_R^2) \sin^2 \theta^*$$

$$|M_b(TR)|^2 = |M_b(+)|^2 + |M_b(-)|^2$$

$$|M_b(LO)|^2 = |M_b(0)|^2$$
(15)
(16)

$$|M_b(LO)|^2 = |M_b(0)|^2 (17)$$

By measuring the polar angle distributions of the Z decay products one can directly determine the differential cross sections for fixed Z helicities. In other words, Z helicity states are obtained from a fit to these distributions. Complete factors $(1/32\pi\Gamma_Z)|M_b(\lambda_Z)|^2$ in front of $d\sigma_1(\lambda_Z)$ in differential cross sections are plotted in Fig.1. As can be seen from Fig.1 longitudinal(LO) and transverse (TR) distributions are well separated from each other. This is why we consider only transverse and longitudinal polarizations for the Z boson in next sections.

INITIAL STATE ELECTROMAGNETIC RADIATIVE CORRECTION III.

Due to small mass of the electron, a significant role is played by the electromagnetic radiative corrections to the initial electron-positron state epecially at linear collider energies. In this work we use structure function formalism to describe the electromagnetic radiative corrections in e^+e^- colliders [7]. The cross section can be written in the following form within this formalism

$$\sigma(s) = \int dx_1 \int dx_2 \ D_1(x_1, Q^2) \ D_2(x_2, Q^2) \sigma'(s') \tag{18}$$

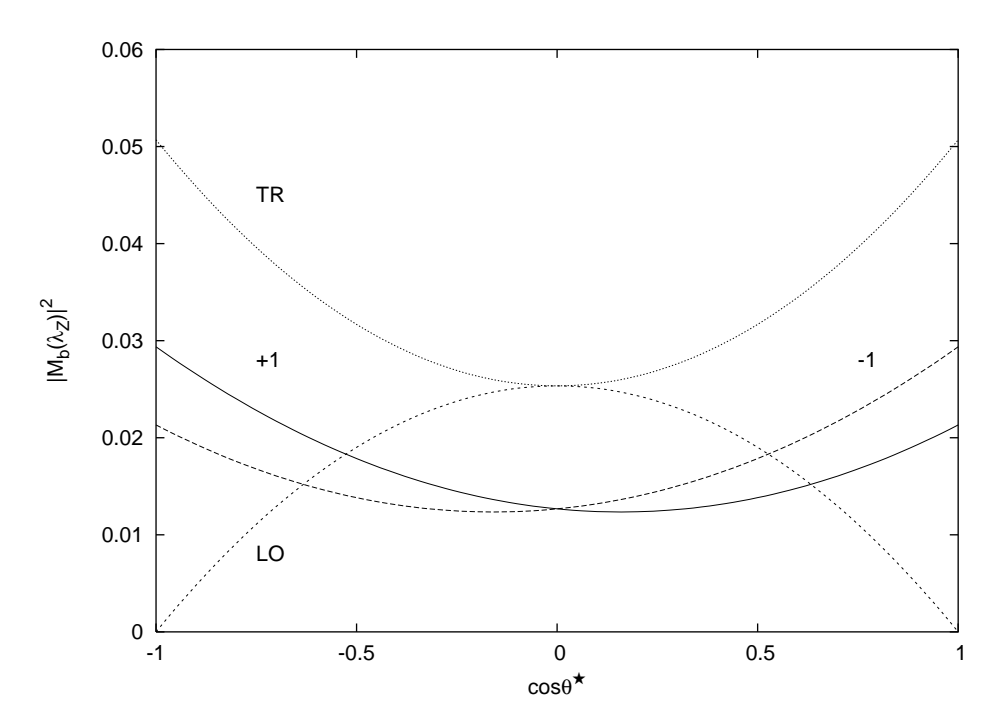


FIG. 1: Polar angle distributions of Z decay product $(1/32\pi\Gamma_Z)|M_b(\lambda_Z)|^2$ in the rest frame of Z boson for $\lambda_Z=-1,+1,0$. Transverse polarization state is defined as the sum of +1 and -1 states.

where $\sigma'(s')$ is the cross section with reduced energy $s' = x_1 x_2 s$. $D_1(x_1, Q^2)$ $(D_2(x_2, Q^2))$ stands for the electron (positron) structure function giving the probability of finding an electron (positron) within an electron (positron) with a longitudinal momentum fraction x_1 (x_2) . Although several definitions of the structure functions are present we use the following ones which are used by HERWIG [8]

$$D_1(x,s) = \beta (1-x)^{\beta-1} g(x,s)$$
(19)

$$g(x,s) = e^{\beta(1+x/2)x/2} (1-\beta^2 \frac{\pi^2}{12}) + y \frac{\beta^2}{8} y [(1+x)\{(1+x)^2 + 3\log x\} - \frac{4\log x}{1-x}]$$
 (20)

$$\beta = \frac{\alpha_{em}}{\pi} (\log \frac{s}{M_c^2} - 1) , \quad y = [\beta (1 - x)^{\beta - 1}]^{-1}$$
 (21)

To avoid divergency at the upper limit of the momentum fraction, x = 1, the cross section can be transformed into different form

$$\sigma(s) = \int_{0}^{1-\epsilon} dx_{1} \int_{0}^{1-\epsilon} dx_{2} D_{1}(x_{1}, s) D_{2}(x_{2}, s) \sigma'(s')
+ \epsilon^{\beta} g_{2}(1, s) \int_{0}^{1-\epsilon} dx_{2} D_{1}(x_{1}, s) \sigma'(x_{1}s) + \epsilon^{\beta} g_{1}(1, s) \int_{0}^{1-\epsilon} dx_{2} D_{2}(x_{2}, s) \sigma'(x_{2}s)
+ \epsilon^{2\beta} g_{1}(1, s) g_{2}(1, s) \sigma'(s)$$
(22)

where ϵ can be taken as $10^{-9} - 10^{-12}$. In this region of ϵ the cross section changes by a factor of 0.985. If one takes smaller ϵ values, higher machine precision gives softer ϵ dependence. The following transformation gives relatively smooth integrand

$$\int_{0}^{1-\epsilon} dx_1 \int_{0}^{1-\epsilon} dx_2 \ D_1(x_1, s) \ D_2(x_2, s) \sigma'(s') = \int_{E_{min}}^{E_{max}} dE \int_{F_{min}}^{F_{max}} dF \ g_1(x_1, s) \ g_2(x_2, s) \sigma'(x_1 x_2 s)$$
(23)

$$x_1 = 1 - (-F)^{1/\beta}, \quad x_2 = 1 - (-E)^{1/\beta}$$
 (24)

$$E_{min} = -\left(1 - \frac{\tau_{min}}{1 - \epsilon}\right), \quad E_{max} = -\epsilon^{\beta} \tag{25}$$

$$F_{min} = -\left(1 - \frac{\tau_{min}}{x_2}\right), \quad F_{max} = -\epsilon^{\beta} \tag{26}$$

$$\tau_{min} = \frac{M_Z^2}{s} \tag{27}$$

Using above formalism we calculate the cross section with initial state radiative corrections for both Standard Model and anomalous coupling cases. In Fig.2 the effects of ISR to the total cross section for the standard model process $e^+e^- \to \gamma Z$ are shown as a function of energy \sqrt{s} (before ISR) with transverse(TR) and longitudinal(LO) Z polarization. Here average over initial spins and sum over photon polarization are performed. The unpolarized cross section is almost the same as the TR polarization case since the magnitude of the cross section is dominated by the cross section with TR polarization. As can be seen from the figures, ISR increases the cross section with a factor 2-3 for the TR case and a factor of 10-100 for LO polarization case depending on the energy. Furthermore, very small LO cross section becomes sizable due to ISR. The reason for this comes from the fact that the energy dependences of the LO and TR cross sections are different. In order to understand this feature let us write standard model squared amplitudes for transverse and longitudinal Z polarizations using the helicity amplitudes given in the appendix

$$|M_a(TR)|^2 = 8[(C_3^L)^2 + (C_3^R)^2](\frac{2}{\sin^2 \theta} - 1)\frac{(m_Z^4 + s^2)}{(s - m_Z^2)^2}$$
(28)

$$|M_a(LO)|^2 = 16[(C_3^L)^2 + (C_3^R)^2] \frac{m_Z^2 s}{(s - m_Z^2)^2}$$
(29)

where $M_a(\lambda_Z)$ is defined in Eq.(8) and we neglect electron mass. As can be seen here the longitudinal part is independent of the polar angle whereas the transverse part strongly depends on it. Angular integration implies that contribution of the transverse polarization always gives larger cross section than the longitudinal one. In both cases, the largest cross section comes from the energy region where $\sqrt{s} \simeq m_Z$. When we consider ISR, the major contribution from the integration over x_1 and x_2 to the cross section is due to the lower limit of the $s' = x_1 x_2 s \simeq m_Z^2$. In this limit the above amplitudes take the forms

$$|M_a(TR)|^2 \simeq 16[(C_3^L)^2 + (C_3^R)^2](\frac{2}{\sin^2 \theta} - 1)\frac{m_Z^4}{(\Delta s)^2}$$
 (30)

$$|M_a(LO)|^2 \simeq 16[(C_3^L)^2 + (C_3^R)^2] \frac{m_Z^4}{(\Delta s)^2}$$
 (31)

where we use $s=m_Z^2+\Delta s$ with $\Delta s<< m_Z^2$. The cross section without ISR leads to s'=s with $x_1=x_2=1$. For the collider energy $\sqrt{s}=1$ TeV where $s >> m_Z^2$ the amplitudes becomes

$$|M_a(TR)|^2 \simeq 8[(C_3^L)^2 + (C_3^R)^2](\frac{2}{\sin^2\theta} - 1)(1 + 2\frac{m_Z^2}{s})$$
 (32)

$$|M_a(LO)|^2 \simeq 16[(C_3^L)^2 + (C_3^R)^2] \frac{m_Z^2}{s}$$
 (33)

Here the LO cross section continiously decreases as s increases. This is the expected result for longitudinal polarization. Because there is no LO polarization for masless vector bosons. For $\sqrt{s} = 10m_Z$ the effect of ISR on both amplitudes can be compared easily as below:

$$\frac{|M_a(TR)|_{ISR}^2}{|M_a(TR)|^2} \simeq \frac{2m_Z^4}{(\Delta s)^2}$$
 (34)

$$\frac{|M_a(LO)|_{ISR}^2}{|M_a(LO)|^2} \simeq 50 \frac{2m_Z^4}{(\Delta s)^2} \tag{35}$$

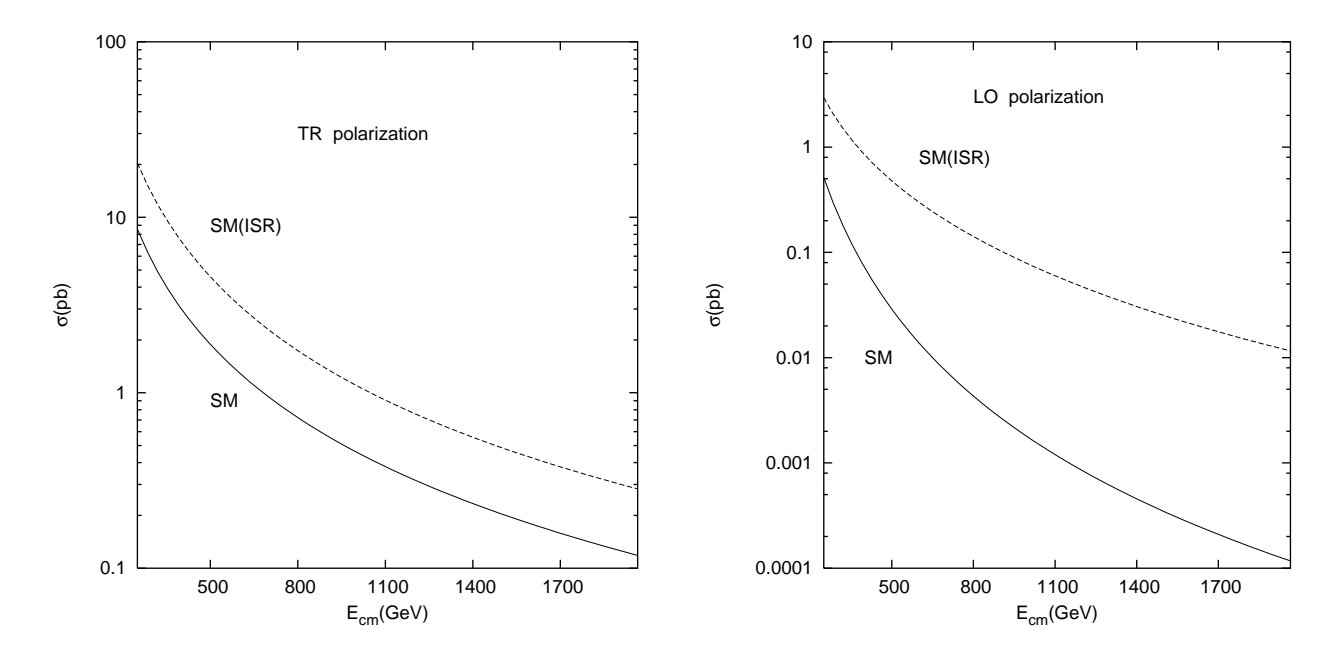


FIG. 2: Effect of ISR to the standard model cross section for $e^+e^- \to \gamma Z$ with transverse and longitudinal polarization of Z boson. Two polarization states, TR and LO, get different contributions from ISR.

Fig.3 shows the energy dependence of the total cross sections with anomalous coupling parameter $h_3^Z=0.01$ for TR and LO polarization states. The contributions of anomalous couplings become remarkably important after the center of mass energy 500-600 GeV. Effect of ISR is also shown for two cases. In the case of LO polarization, after the energy of 900 GeV the ISR gives negligible corrections. Similar behaviour appears for $h_3^{\gamma}=0.01$ and $h_4^Z=h_4^{\gamma}=0.001$ values. In Fig.4 the energy dependences of the ISR corrected total cross sections with four anomalous coupling parameters are plotted for LO polarization and unpolarized cases.

It is also important to see how the anomalous couplings change the shape of the angular distribution of the Z boson for the polarized and unpolarized cases. Angular distribution of the Z boson is shown in Fig. 5 for LO polarization state with and wihout ISR correction. Since the TR polarization state of the Z boson is poorly sensitive to anomalous couplings, angular distributions with TR case are not plotted. In all figures, only one of the coupling parameters are kept different from zero. From all these figures we reach at the following remarkable results. The LO polarization states are always more sensitive to the anomalous couplings. Much larger deviations arise from h_4^V for both TR and LO polarizations. $Z\gamma\gamma^*$ couplings always provide the higher contribution to the cross section than the $Z\gamma Z^*$ couplings. The shape of the curves differs for two kinds of polarizations of the Z boson. The ISR correction gives larger contribution to the SM cross section than the case with anomalous couplings. Therefore, the sensitivity of the $e^+e^- \to \gamma Z$ process to the anomalous couplings is expected to become poorer due to the ISR correction. Numerical results for all polarization configurations will be given in the next section.

IV. LIMITS ON THE ANOMALOUS COUPLING PARAMETERS

If the Z boson decays into a pair of charged leptons the signal for the final states can be $\gamma \ell \ell$ where we consider $\ell = e, \mu$. The potential background processes for $\ell = \mu$ final state are the following:

 $e^+e^- \to Z(\gamma) \to \gamma \ell \ell$: s channel Z or γ exchange (final state bremstrahlung).

 $e^+e^- \to \gamma\gamma \to \gamma\ell\ell$: t channel e exchange.

For $\ell = e$ final state additional t channel background processes such as those arising from both $Z(\gamma)$ and e exchange; Z or γ exchange (final state bremstrahlung) are present. Since we take into account only on shell Z bosons, we should impose a cut on the invariant mass of charged leptons $M_{\ell\ell} \simeq M_Z$. This cut reduces the effect of background processes

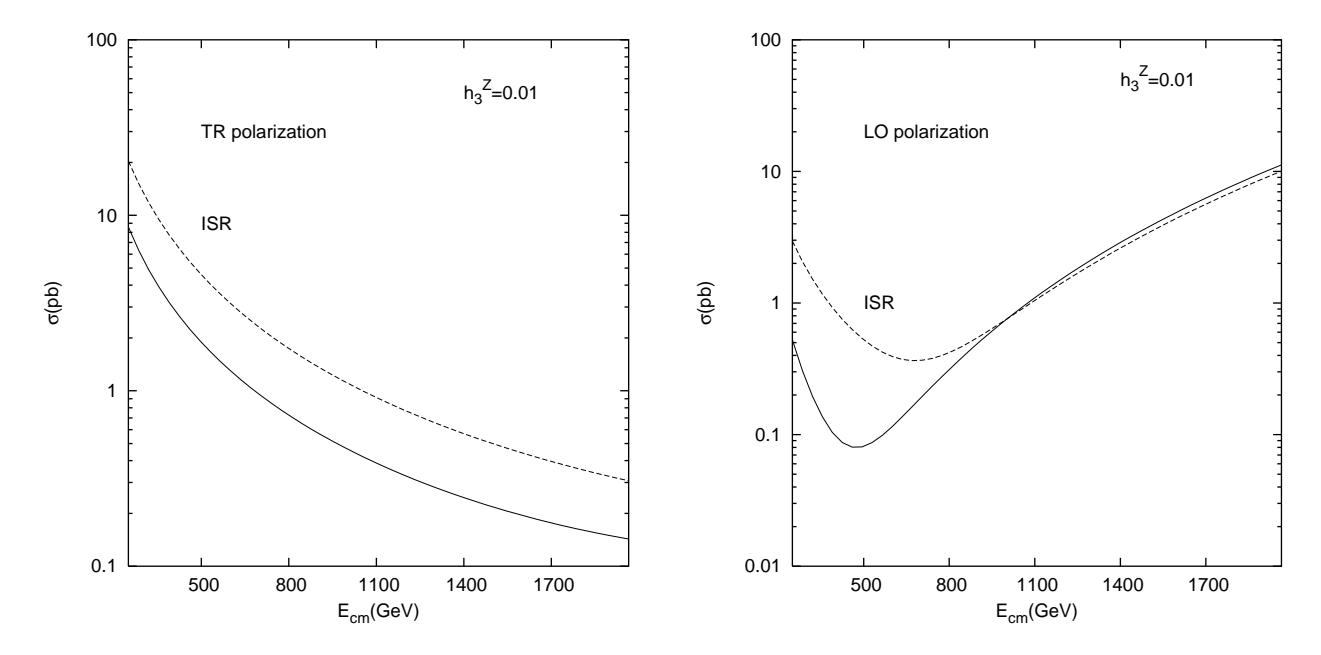


FIG. 3: Energy dependence of the total cross section for $e^+e^- \to \gamma Z$ with anomalous $ZZ\gamma$ vertex parameter $h_3^Z=0.01$. Effects of ISR and Z polarization are also shown. As in the previous figure, two polarization states of the Z boson get different contributions from ISR.

for $\ell = \mu$ drastically. The total cross section of background processes at least 100 times smaller than the process $e^+e^- \to Z\gamma \to \gamma\ell\ell$ (t channel e exchange with on shell Z boson). In the case of $\ell=e$ final state background cross sections are 10 times higher when compared to μ final states. Therefore the major potential background is due to $\ell=e$ final states. In the following sensitivity calculation, background contributions have a negligible effect. In order to obtain realistic limits on the h_3^V and h_4^V from the linear e^+e^- collider the number of events have been calculated using $N = A\sigma(e^+e^- \to \gamma Z)BR(Z \to \ell^+\ell^-)L_{int}$ for integrated luminosity $L_{int} = 500fb^{-1}$. Here lepton channel of the Z decay and overall acceptance A=0.85 has been taken into account. For total cross section $|\cos \theta| = 0.99$ has been used as angular region. The 95% confidence level (C.L.) limits have been estimated from total cross section using simple one parameter χ^2 test for \sqrt{s} =0.5, 1, 1.5 TeV. At \sqrt{s} = 1.5 TeV the SM cross section without ISR correction gives the smallest number of events N=40 (using the above formula) for LO polarization state. If ISR correction is included number of events increases up to N=2800. For lower initial energy, $\sqrt{s}=1$ TeV, the smallest event number becomes 250 and 10000 without and with ISR correction. The limits which have been obtained are shown in Tables I-III for the deviation of the cross section from the standard model value without systematic error. It should be noted that better limits are obtained for the polarization configuration λ_Z =LO which leads to the order of O(10⁻³ – 10⁻⁴) for h_3^Z and h_3^γ , O(10⁻⁴ – 10⁻⁶) for h_4^Z and h_4^γ at $\sqrt{s}=0.5-1.5$ TeV when ISR corrections are taken into account. Without ISR correction, the LO polarization of the Z boson improves the limits by factors 3-7 depending on the energy. The LO polarization with ISR correction improves the limits by factors 2-2.5 which should be taken as the realistic results. As can be seen from the tables, TR polarizations are not sensitive to anomalous couplings. But the advantage of TR polarization case is the absence of h_4^Z and h_4^{γ} couplings. This feature reduces the number of coupling parameters. In order to see the degree of energy dependence on the anomalous couplings let us take into account the increase in c.m. energy from 0.5 TeV to 1.5 TeV for the LO polarization configuration. Then we get the improvements in sensitivity limits by a factor 20, 30 for h_3^Z and h_3^{γ} , by a factor 150, 200 for h_4^Z and h_4^{γ} .

V. CONCLUSION

Future linear e^+e^- colliders with $\sqrt{s} = 0.5 - 1.5$ TeV energy and integrated luminosity $500fb^{-1}$ probe the $Z\gamma Z^*$ and $Z\gamma\gamma^*$ anomalous couplings with far better sensitivity than the present colliders Fermilab Tevatron and LEP2 experiments. Measurement of final state Z boson polarization is important in two ways. First, LO polarization state is always far more sensitive to anomalous couplings. Second, TR polarization state contains only h_3^Z and h_3^γ . Initial

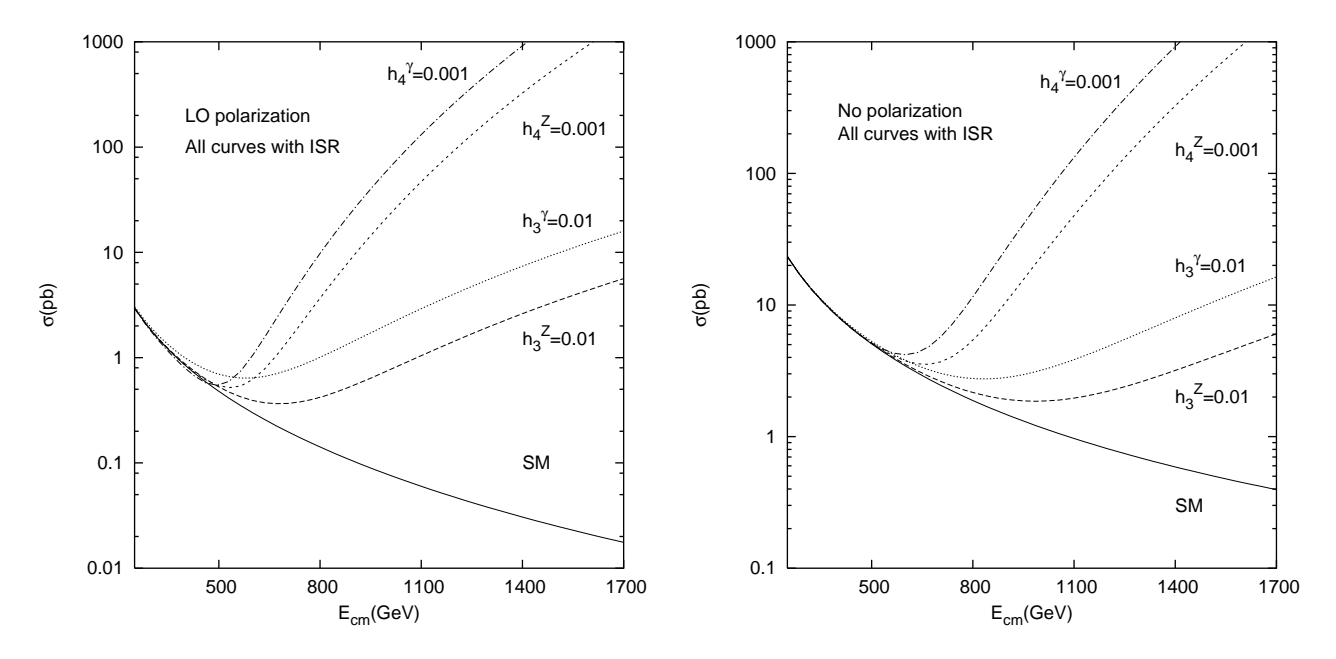


FIG. 4: Energy dependence of the total cross section for $e^+e^- \to \gamma Z$ with LO polarization (left) and unpolarized (right) cases. The values of the anomalous $ZZ\gamma$ and $Z\gamma\gamma$ vertex parameters $h_3^Z=h_3^\gamma=0.01$ and $h_4^Z=h_4^\gamma=0.001$ are chosen. All cross sections are ISR corrected.

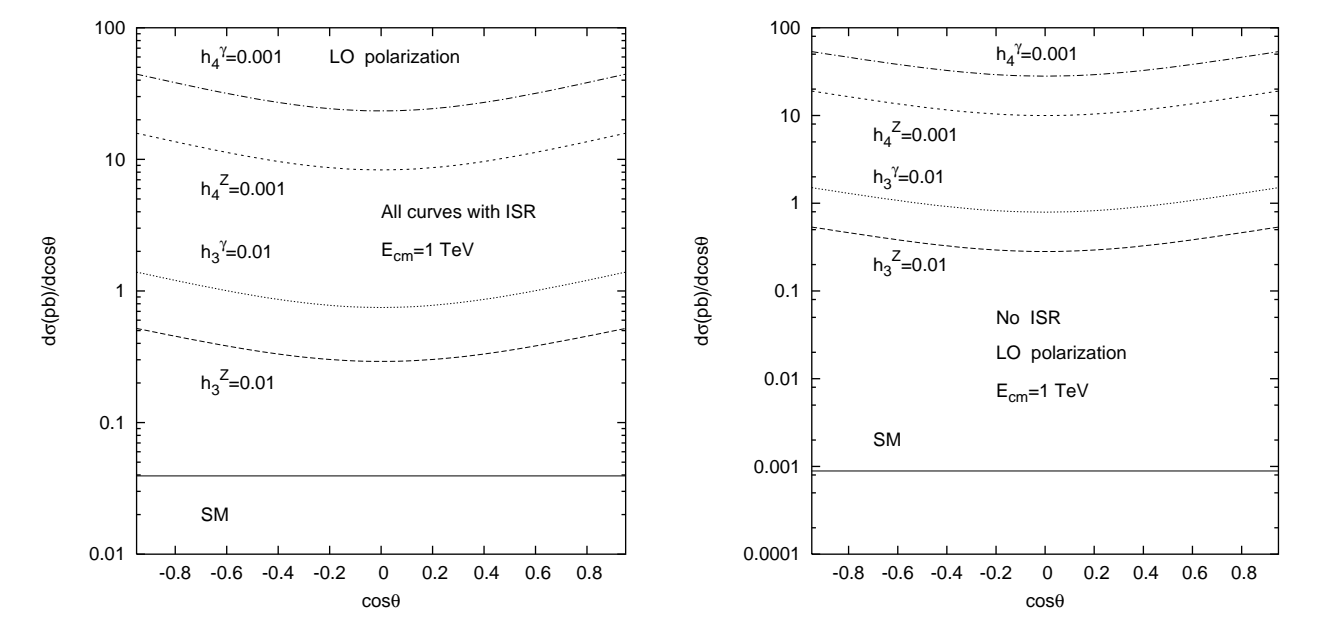


FIG. 5: Angular distributions of the outgoing Z boson in the center of mass frame of outgoing Z and the photon. θ is the angle between the outgoing Z boson and the incoming electron. Angular dependence of the four anomalous couplings are shown with (left) and without(right) ISR corrections. Only LO polarization states are taken into account in these figures since TR polarization states are poorly sensitive to anomalous couplings.

TABLE I: Sensitivity of the linear e^+e^- collider to $ZZ\gamma$ and $Z\gamma\gamma$ couplings at 95% C.L. for $\sqrt{s}=0.5$ TeV and $L_{int}=500$ fb^{-1} . Only one of the couplings is assumed to deviate from the SM at a time.

λ_Z	h_3^Z	h_4^Z	h_3^{γ}	h_4^{γ}
TR+LO	$ 6 \times 10^{-3} $	$ 4 \times 10^{-4} $	$ 4 \times 10^{-3} $	$ 2 \times 10^{-4} $
(ISR)	$ 8 \times 10^{-3} $	$ 6 \times 10^{-4} $	$ 5 \times 10^{-3}$	$ 3 \times 10^{-4} $
TR	$ 3 \times 10^{-2} $	-	$ 2 \times 10^{-2} $	-
(ISR)	$ 4 \times 10^{-2} $	-	$ 3 \times 10^{-2} $	-
LO	$ 2 \times 10^{-3} $	$ 1 \times 10^{-4} $	$ 1 \times 10^{-3} $	$ 8 \times 10^{-5} $
(ISR)	$ 4\times10^{-3} $	$ 3 \times 10^{-4} $	$ 3 \times 10^{-3} $	$ 2\times10^{-4} $

TABLE II: Sensitivity of the linear e^+e^- collider to $ZZ\gamma$ and $Z\gamma\gamma$ couplings at 95% C.L. for $\sqrt{s}=1$ TeV and $L_{int}=500~fb^{-1}$. Only one of the couplings is assumed to deviate from the SM at a time.

λ_Z	h_3^Z	h_4^Z	h_3^{γ}	h_4^{γ}
TR+LO	$ 1 \times 10^{-3} $	$ 2 \times 10^{-5} $	$ 6 \times 10^{-4} $	$ 1 \times 10^{-5} $
(ISR)	$ 1 \times 10^{-3} $	$ 2 \times 10^{-5} $	$ 8 \times 10^{-4} $	$ 1 \times 10^{-5} $
TR	$ 1 \times 10^{-2} $	-	$ 7 \times 10^{-3} $	-
(ISR)	$ 1 \times 10^{-2} $	-	$ 8 \times 10^{-3} $	-
LO	$ 3 \times 10^{-4} $	$ 4 \times 10^{-6} $	$ 2 \times 10^{-4} $	$ 3 \times 10^{-6} $
(ISR)	$ 7 \times 10^{-4} $	$ 1\times10^{-5} $	$ 4\times10^{-4} $	$ 7 \times 10^{-6} $

state electromagnetic radiative correction improves the number of events especially for the Standard Model processes at the linear collider energies. Furthermore, LO polarization case gets larger contribution from the ISR than the case of TR polarization.

Some limits on the above couplings via $e^+e^- \to Z\gamma$ process at linear collider energies from similar works are the following for comparison: the sensitivity (one standard deviation) 2×10^{-4} , 4×10^{-3} , 4×10^{-5} , 3×10^{-4} for h_3^γ , h_4^Z , h_4^γ , h_4^Z , respectively at 500 GeV energy and 100 fb^{-1} luminosity [9]; the sensitivity(95% C.L.) $O(10^{-2})$ for h_3^γ , h_3^Z , $O(10^{-3})$ for h_4^γ , h_4^Z at 500 GeV and 10 fb^{-1} [10]. Predictions from CERN LHC [2] give the limits 5.2×10^{-3} , 3.7×10^{-5} for h_3^Z and h_4^Z at 2σ , 10 fb^{-1} . Comparison of the results in this work at $\sqrt{s}=1.5$ TeV with those of LHC shows that our results are improved one order of magnitude. For more precise results, further analysis needs to be supplemented with a more detailed knowledge of the experimental conditions.

TABLE III: Sensitivity of the linear e^+e^- collider to $ZZ\gamma$ and $Z\gamma\gamma$ couplings at 95% C.L. for $\sqrt{s}=1.5$ TeV and $L_{int}=500$ fb^{-1} . Only one of the couplings is assumed to deviate from the SM at a time.

λ_Z	h_3^Z	h_4^Z	h_3^{γ}	h_4^{γ}
TR+LO	$ 4 \times 10^{-4} $	$ 3 \times 10^{-6} $	$ 2 \times 10^{-4} $	$ 2 \times 10^{-6} $
(ISR)	$ 5 \times 10^{-4} $	$ 4 \times 10^{-6} $	$ 3 \times 10^{-4} $	$ 2 \times 10^{-6} $
TR	$ 6 \times 10^{-3} $	-	$ 4 \times 10^{-3} $	-
(ISR)	$ 7 \times 10^{-3} $	-	$ 4 \times 10^{-3} $	-
LO	$ 7 \times 10^{-5} $	$ 5 \times 10^{-7} $	$ 4 \times 10^{-5} $	$ 3 \times 10^{-7} $
(ISR)	$ 2 \times 10^{-4} $	$ 2 \times 10^{-6} $	$ 1 \times 10^{-4} $	$ 1 \times 10^{-6} $

^[1] F.M. Renard, Nucl. Phys. **B196**, 93 (1982);

 ^[2] U. Baur and E. L. Berger, Phys. Rev. **D47**, 4889 (1993);
 K. Hagiwara *et al.*, Nucl. Phys. **B282**, 253 (1987);

- [3] C. N. Yang, Phys. Rev. 77, 242 (1950).
- [4] D0 Collaboration, B. Abbott et al. Phys. Rev. D57, R3817 (1998);
 D0 Collaboration, S. Abachi et al. Phys. Rev. Lett. 75, 1028 (1995);
- D0 Collaboration, S. Abachi *et al.* Phys. Rev. Lett. **78**, 3640 (1997). [5] The LEP Electroweak Working Group, CERN-EP/2003-XXX;

The OPAL Collaboration, Eur. Phys. J. C17, 553 (2000);

L3 Collaboration, M. Acciarri et al., Phys. Lett **B436**, 187 (1998);

L3 Collaboration, M. Acciarri et al., Phys. Lett B346, 190 (1995);

DELPHI Collaboration, P. Abreu et al., Phys. Lett. B380, 471 (1996).

- [6] U. Baur and D. Rainwater, Int. J. Mod. Phys. A16S1A, 315 (2001);
 - U. Baur and D. Rainwater, Phys. Rev. **D62**, 113011 (2000).
- [7] E.A. Kuraev, V.S. Fadin, Sov. J. Nucl. Phys. 41, 466 (1985);
 - G. Alterelli, G. Martinelli, in *Physics at LEP*, J. Ellis, R. Peccei eds. CERN 86-02 (CERN, Geneva, 1986);
 - O. Nicrosini, L. Trentadue, Phys. Lett. **B196**, 551 (1987); Z. Phys. **C39**, 479 (1988);
 - F.A. Berends, G. Burgers, W.L. van Neerven, Nucl. Phys. **B297**, 429 (1988).
- [8] G. Alterelli, T. Sjstrand and F. Zwirner eds., Physics at LEP2, vol.2 p139, CERN yellow report 96-01.
- [9] G.J. Gounaris, J. Layssac and F.M. Renard, Phys. Rev. **D62**, 073012 (2000).
- [10] R. Walsh and A.J. Ramalho, Phys. Rev. **D57**, 5908 (1998).
- [11] SLD Collaboration, K. Abe et al., Phys. Rev. Lett. 86 1162 (2001); SLD Collaboration, K. Abe et al., Phys. Rev. Lett. 79 804 (1997).

APPENDIX: HELICITY AMPLITUDES

There are four Feynman diagrams for the process $e^+e^- \to Z\gamma$ if one includes $Z\gamma Z^*$, $Z\gamma\gamma^*$ vertices. Helicity amplitudes M_1 and M_2 are responsible for the diagrams concerning $Z\gamma Z^*$ and $Z\gamma\gamma^*$ interactions arising from s channel Z or γ exchanges. M_3 and M_4 are standard model contribution of the t and u channel of the process. The parameters of the helicity amplitudes $M(\sigma_e, \sigma'_e; \lambda_Z, \lambda_\gamma)$ are helicities of incoming electron and positron, outgoing Z boson and photon. The values they take are given by:

$$\sigma_e : L, R , \sigma'_e : L, R , \lambda_Z : +, -, 0 , \lambda_{\gamma} : +, -$$
 (A.1)

Here L and R stand for left and right. Helicity amplitudes we have obtained for each Feynman diagram in the c.m. frame of e^+e^- can be written as follows:

$$M(\sigma_e, \sigma'_e; \lambda_Z, \lambda_\gamma) = M_1(\sigma_e, \sigma'_e; \lambda_Z, \lambda_\gamma) + M_2(\sigma_e, \sigma'_e; \lambda_Z, \lambda_\gamma) + M_3(\sigma_e, \sigma'_e; \lambda_Z, \lambda_\gamma) + M_4(\sigma_e, \sigma'_e; \lambda_Z, \lambda_\gamma)$$
(A.2)

$$M_1(LR; ++) = -C_1^L h_3^Z (M_Z^2 - s) \sin \theta \tag{A.3}$$

$$M_1(RL; ++) = -C_1^R h_3^Z (M_Z^2 - s) \sin \theta$$
(A.4)

$$M_1(LR; +-) = 0$$
 (A.5)

$$M_1(RL; +-) = 0$$
 (A.6)

$$M_1(LR; --) = C_1^L h_3^Z (M_Z^2 - s) \sin \theta$$
 (A.7)

$$M_1(RL; --) = -C_1^R h_3^Z (M_Z^2 - s) \sin \theta$$

$$M_1(LR; -+) = 0$$
(A.8)

$$M_1(RL; -+) = 0$$
 (A.10)

$$M_1(LR; 0+) = -\frac{C_1^L}{\sqrt{2}M_Z}\sqrt{s}(M_Z^2 - s)(1 + \cos\theta) \left[h_3^Z + \frac{(M_Z^2 - s)h_4^Z}{2M_Z^2}\right]$$
(A.11)

$$M_1(RL; 0+) = \frac{C_1^R}{\sqrt{2}M_Z} \sqrt{s} (M_Z^2 - s)(1 - \cos\theta) \left[h_3^Z + \frac{(M_Z^2 - s)h_4^Z}{2M_Z^2} \right]$$
(A.12)

$$M_1(LR; 0-) = \frac{C_1^L}{\sqrt{2}M_Z} \sqrt{s} (M_Z^2 - s)(1 - \cos \theta) \left[h_3^Z + \frac{(M_Z^2 - s)h_4^Z}{2M_Z^2} \right]$$
 (A.13)

$$M_1(RL;0-) = -\frac{C_1^R}{\sqrt{2}M_Z}\sqrt{s}(M_Z^2 - s)(1 + \cos\theta) \left[h_3^Z + \frac{(M_Z^2 - s)h_4^Z}{2M_Z^2}\right]$$
(A.14)

where

$$C_1^L = \frac{g_e g_L}{2M_Z^2} , \quad C_1^R = \frac{g_e g_R}{2M_Z^2}$$
 (A.15)

with

$$g_L = \frac{g_Z}{2}(C_V + C_A) , \quad g_R = \frac{g_Z}{2}(C_V - C_A)$$
 (A.16)

$$C_V = 2\sin^2\theta_W - \frac{1}{2} , \quad C_A = -\frac{1}{2}$$
 (A.17)

$$g_Z = \frac{g_e}{\sin \theta_W \cos \theta_W} , \quad g_e^2 = 4\pi\alpha$$
 (A.18)

$$M_2(LR; ++) = -C_2 h_3^{\gamma} (M_Z^2 - s) \sin \theta \tag{A.19}$$

$$M_2(RL; ++) = M_2(LR; ++)$$
 (A.20)

$$M_2(LR; +-) = 0$$
 (A.21)

$$M_2(RL; +-) = 0$$
 (A.22)

$$M_2(LR; -+) = 0 \tag{A.23}$$

$$M_2(RL; -+) = 0 (A.24)$$

$$M_2(LR; --) = C_2 h_3^{\gamma}(M_Z^2 - s) \sin \theta$$
 (A.25)

$$M_2(RL; --) = M_2(LR; --)$$
 (A.26)

$$M_2(LR; 0+) = -\frac{C_2}{\sqrt{2}M_Z}\sqrt{s}(M_Z^2 - s)(1 + \cos\theta) \left[h_3^{\gamma} + \frac{(M_Z^2 - s)h_4^{\gamma}}{2M_Z^2}\right]$$
(A.27)

$$M_2(RL; 0+) = \frac{C_2}{\sqrt{2}M_Z} \sqrt{s} (M_Z^2 - s)(1 + \cos \theta) \left[h_3^{\gamma} + \frac{(M_Z^2 - s)h_4^{\gamma}}{2M_Z^2} \right]$$
(A.28)

$$M_2(LR; 0-) = M_2(RL; 0+)$$
 (A.29)

$$M_2(RL; 0-) = M_2(LR; 0+)$$
 (A.30)

$$C_2 = \frac{Q_e g_e^2}{2M_Z^2} \,, \quad , \quad Q_e = -1$$
 (A.31)

$$M_3(LR; ++) = -\frac{C_3^L s(1 - \cos \theta) \sin \theta}{2M_e^2 + (s - M_Z^2)(1 - \cos \theta)}$$
(A.32)

$$M_3(RL; ++) = \frac{C_3^R [2M_Z^2 - s(1 - \cos \theta)] \sin \theta}{2M_e^2 + (s - M_Z^2)(1 - \cos \theta)}$$
(A.33)

$$M_3(LR; +-) = \frac{C_3^L s(1 - \cos \theta) \sin \theta}{2M_e^2 + (s - M_Z^2)(1 - \cos \theta)}$$
(A.34)

$$M_3(RL; +-) = -\frac{C_3^R s(1 + \cos \theta) \sin \theta}{2M_e^2 + (s - M_Z^2)(1 - \cos \theta)}$$
(A.35)

$$M_3(LR; --) = \frac{C_3^L[2M_Z^2 - s(1 - \cos\theta)]\sin\theta}{2M_e^2 + (s - M_Z^2)(1 - \cos\theta)}$$
(A.36)

$$M_3(RL; --) = -\frac{C_3^R s(1 - \cos \theta) \sin \theta}{2M_s^2 + (s - M_Z^2)(1 - \cos \theta)}$$
(A.37)

$$M_3(LR; -+) = -\frac{C_3^L s(1 + \cos \theta) \sin \theta}{2M_e^2 + (s - M_Z^2)(1 - \cos \theta)}$$
(A.38)

$$M_3(RL; -+) = \frac{C_3^R s(1 - \cos\theta) \sin\theta}{2M_e^2 + (s - M_Z^2)(1 - \cos\theta)}$$
(A.39)

$$M_3(LR; 0+) = -\frac{C_3^L \sqrt{s(s+M_Z^2)} \sin^2 \theta}{\sqrt{2} M_Z [2M_e^2 + (s-M_Z^2)(1-\cos \theta)]}$$
(A.40)

$$M_3(RL; 0+) = -\frac{C_3^R \sqrt{2s} [3M_Z^2 - s + (s + M_Z^2) \cos \theta] \sin^2 \frac{\theta}{2}}{M_Z[2M_e^2 + (s - M_Z^2)(1 - \cos \theta)]}$$
(A.41)

$$M_3(LR; 0-) = \frac{C_3^L \sqrt{2s} [3M_Z^2 - s + (s + M_Z^2) \cos \theta] \sin^2 \frac{\theta}{2}}{M_Z[2M_e^2 + (s - M_Z^2)(1 - \cos \theta)]}$$
(A.42)

$$M_3(RL; 0-) = \frac{C_3^R \sqrt{s(s+M_Z^2)} \sin^2 \theta}{\sqrt{2} M_Z [2M_z^2 + (s-M_Z^2)(1-\cos \theta)]}$$
(A.43)

$$C_3^L = Q_e g_e g_L \; , \quad C_3^R = Q_e g_e g_R$$
 (A.44)

$$M_4(LR; ++) = \frac{C_4^L[s(1+\cos\theta) - 2M_Z^2]\sin\theta}{2M_e^2 + (s-M_Z^2)(1+\cos\theta)}$$
(A.45)

$$M_4(RL; ++) = \frac{C_4^R s(1 + \cos \theta) \sin \theta}{2M_e^2 + (s - M_Z^2)(1 + \cos \theta)}$$
(A.46)

$$M_4(LR; +-) = \frac{C_4^L s(1 - \cos \theta) \sin \theta}{2M_e^2 + (s - M_Z^2)(1 + \cos \theta)}$$
(A.47)

$$M_4(RL; +-) = -\frac{C_4^R s(1 + \cos \theta) \sin \theta}{2M_e^2 + (s - M_Z^2)(1 + \cos \theta)}$$
(A.48)

$$M_4(LR; --) = \frac{C_4^L s(1 + \cos \theta) \sin \theta}{2M_e^2 + (s - M_Z^2)(1 + \cos \theta)}$$
(A.49)

$$M_4(RL; --) = \frac{C_4^R[s(1+\cos\theta) - 2M_Z^2]\sin\theta}{2M_e^2 + (s-M_Z^2)(1+\cos\theta)}$$
(A.50)

$$M_4(LR; -+) = -\frac{C_4^L s(1 + \cos \theta) \sin \theta}{2M_e^2 + (s - M_Z^2)(1 + \cos \theta)}$$
(A.51)

$$M_4(RL; -+) = \frac{C_4^R s(1 - \cos\theta) \sin\theta}{2M_e^2 + (s - M_Z^2)(1 + \cos\theta)}$$
(A.52)

$$M_4(LR; 0+) = \frac{C_4^L \sqrt{2s} [s + (s + M_Z^2) \cos \theta - 3M_Z^2] \cos^2 \frac{\theta}{2}}{M_Z [2M_e^2 + (s - M_Z^2)(1 + \cos \theta)]}$$
(A.53)

$$M_4(RL; 0+) = -\frac{C_4^R \sqrt{s(s+M_Z^2)} \sin^2 \theta}{\sqrt{2} M_Z [2M_e^2 + (s-M_Z^2)(1+\cos \theta)]}$$
(A.54)

$$M_4(LR; 0-) = \frac{C_4^L \sqrt{s}(s+M_Z^2) \sin^2 \theta}{\sqrt{2} M_Z [2M_e^2 + (s-M_Z^2)(1+\cos \theta)]}$$
(A.55)

$$M_4(RL; 0-) = -\frac{C_4^R \sqrt{2s} [s + (s + M_Z^2) \cos \theta - 3M_Z^2] \cos^2 \frac{\theta}{2}}{M_Z [2M_e^2 + (s - M_Z^2)(1 + \cos \theta)]}$$
(A.56)

$$C_4^L = C_3^L , \quad C_4^R = C_3^R$$
 (A.57)